Biomimetic Ion-Binding Monolayers on Gold and Their Characterization by AC-Impedance Spectroscopy

Yael Gafni, Haim Weizman, Jacqueline Libman, Abraham Shanzer,* and Israel Rubinstein*

Abstract: Novel ion-binding monolayers on gold surfaces are presented where the molecular design is based upon the natural ion binder ferrichrome. The new ion binders possess hydroxamate coordinating groups arranged in C_2 symmetry (bishydroxamate binder, BHB) or C_3 symmetry (trishydroxamate binder, THB), and a separate dialkyl sulfide moiety, which serves as an anchor to the gold substrate. The separation between the ion-binding cavity and the attachment site to the gold allows each parameter to be controlled separately, namely, cavity size, its symmetry and external envelope, as well as the functional group used for immobilization. The monolayers were characterized with respect to ellipsometric thickness, wettability (advancing and receding contact angles (CAs) for water), and surface coverage; the latter is determined by metal underpotential deposition (UPD). It is shown that the introduction of hydrophobic side chains (*i*-butyl) improves the CAs, thickness, and surface coverage of the monolayers. A detailed analysis of the alternating-current (AC) impedance spectra is presented for THB monolayers on gold electrodes, where the impedance data are fitted to an equivalent circuit model. It is shown that the AC response in a wide frequency range can be used to probe ion binding and release in monolayer systems on electrodes.

Keywords
ionophores · impedance spectroscopy · membrane models · monolayers · self-assembly

Introduction

Understanding the relationships that exist between the chemical composition, structure, and function of cell membranes represents a major challenge presently facing chemistry and biology. The complexity of biological membranes has provided an incentive for numerous studies of model systems. One such model, though largely oversimplified, consists of organized monomolecular films on solid substrates; self-assembled (SA) sulfur-containing monolayers on gold are a prominent example of this type of system.[1] These monolayers have been studied extensively in recent years, owing to their unique structural properties and potential applications, for example, as (primitive) model systems for biological membranes[2] and basic building blocks for future technologies.[1]

In the last few years we have conducted a study of ion-binding SA monolayers on gold electrodes, that is, SA monolayers that bind selected ions in the presence of other ions in solution. Our approach has been to mimic the basic elements found in natural membranes, by incorporating active and blocking monolayer components to provide both blocking and selectivity. The gold electrode serves as a support for the SA monolayer as well as the source of the electrochemical signal required to probe the binding of ions. This approach was used to study ion-selective monolayer membranes comprising "receptor" molecules (e.g. 2,2'-thiobisethylacetoacetate, TBEA) and surface-sealing long-chain amphiphiles (n-octadecylmercaptan (OM) or *n*-octadecyltrichlorosilane (OTS)).[3] Selective response for certain divalent ions, such as Cu^{2+} or Pb^{2+}, was observed in the presence of interfering ions such as Fe^{2+} or Fe^{3+}. The recognition was shown to be based upon selective binding of ions with specific coordination and geometric requirements to the ligand molecules in the monolayer membrane;[3d] binding allowed electron transfer with the gold electrode to occur, which was monitored primarily by voltammetry.

The successful construction of the above systems prompted us to develop a general approach to the preparation of functional monolayers, based upon rational design of the active component. At the heart of this design lies the conceptual separation between the recognition site and the immobilization site of the ion binder, thus offering several advantages over previous systems: 1) The independent design and synthesis of the ion-binding site allows its optimization in solution prior to addition of an immobilization tail. 2) The biomimetic design of the ion-binding cavity relies on the use of naturally occurring iron-binding molecules (siderophores)[4] as guiding models, and thereby provides ion binders that form conformationally well-defined metal complexes of 1:1 stoichiometry.[5] These may therefore be assembled either as the free ligand or as the preformed complex. The latter option is of particular significance, as it allows unambiguous identification of the recognition site in the functional monolayer. In addition, the modular assembly enables systematic variation of ligand symmetry, binding groups, cavity di-

[*] A. Shanzer, H. Weizman, J. Libman
Department of Organic Chemistry, Weizmann Institute of Science
Rehovot 76100 (Israel)
Fax: Int. code +(8)934-4142
e-mail: coshanzr@weizmann.weizmann.ac.il
I. Rubinstein, Y. Gafni
Department of Materials and Interfaces
Weizmann Institute of Science

  0947-6539/96/0207-0759 $ 15.00+.25/0

mensions, and cavity envelope, allowing effective control of the binding properties and monolayer packing.

This paper illustrates the virtues of the modular design by the preparation of two types of ion-binding monolayers: 1) THB (trishydroxamate binders), derived from C_3-symmetric ion binders, suitable for binding Fe^{III};[5a, b] and 2) BHB (bishydroxamate binders), derived from C_2-symmetric ion binders, suitable for binding Cu^{II}.[5d] Both types are constructed from the same building blocks, as shown schematically in Figure 1.

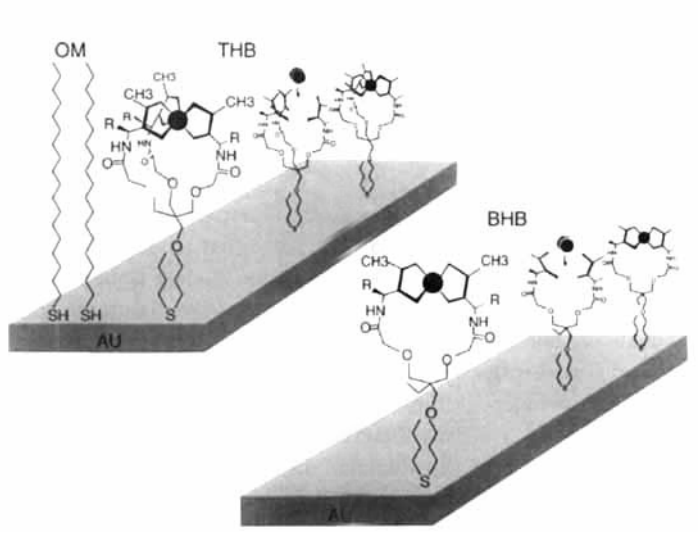

Fig. 1. Schematic representation of THB and BHB monolayers on gold substrates.

We have previously shown that voltammetry provides an effective tool for monitoring the binding of certain ions to monolayer membranes containing TBEA-type ion binders.[3] This technique, however, suffers from two serious limitations: 1) It can be used only with ions that show redox response in the accessible potential range; 2) the heterogeneous electron transfer rate (i.e., electron tunneling between the gold and the bound ion) is usually assumed to decrease exponentially with distance. This would imply that the measured voltammetric response may change substantially upon small changes in the orientation of the monolayer (i.e., small variations in the tilt angle), and the results may be poorly reproducible. Thus, methods based upon electron transfer, such as voltammetry, may not always be the best choice for probing ion binding to ligand molecules in monolayers.

Yet, electrochemical techniques are convenient and relatively simple to apply for sensing, usually more so than optical or surface analysis techniques. We therefore resorted to alternating-current (AC) impedance spectroscopy[6, 7] as a natural choice for our purpose, providing a powerful electrochemical technique that supplies satisfactory solutions to the shortcomings of voltammetry. A similar approach using AC-impedance spectroscopy to study processes in biological membranes was recently reported by Sackmann and co-workers.[8]

The advantages of AC-impedance spectroscopy are manifold:

1) Analysis of impedance data in a wide frequency range provides a complete picture of the electrical properties of the system, including capacitances and resistances, *in the presence or absence of electron transfer processes*.[6, 7]
2) AC-impedance measurements involve the application of a minute voltage perturbation (typically a few mV), thus inducing minimal disturbance to the monolayer; in comparison, voltammetry typically requires voltage variations of hundreds of mV, which may cause modification of the monolayer structure and composition.
3) In the most simple view, the monolayer capacitance would be inversely proportional to the thickness (parallel-plate capacitor), while its resistance would change linearly with the thickness. Hence, both elements are expected to show a much weaker dependence on monolayer orientation than is the case with voltammetry (exponential dependence, see above).

This paper describes the preparation and characterization of ion-binding monolayer membranes comprising the ligands THB and BHB. The use of impedance spectroscopy to follow structural and compositional modifications in SA monolayer systems is demonstrated for the first time.

Experimental Procedure

Chemicals: Octadecylmercaptan (OM) (Aldrich) was recrystallized from hexane. Chloroform (Biolab, AR), bicyclohexyl (BCH) (Aldrich, AR) and hexadecane (HD) (Sigma, AR) were passed through a column of activated basic alumina (Alumina B, Akt. 1, ICN). Ethanol (Merck, AR), H_2O_2 (Frutarom, CP), NaOH (Merck, AR), HNO_3 (Palacid, 69–70%), HCl (Frutarom, 32%), $CuSO_4$ (Merck, AR), Na_2SO_4 (Merck, AR), $Fe_2(SO_4)_3$ (Fluka, AR), acetic acid (Frutarom, AR), sodium acetate (BDH, AR), and EDTA, sodium salt (Baker, AR) were used as received. Gases used were argon (99.996%), oxygen (99.5%), and dry purified air. Water was triply distilled.

Gold electrodes: Optically polished n-type single crystal (100) silicon wafers (National Semiconductor, Israel) were cut into $\approx 22 \times 11$ mm slides. The slides were sonicated in absolute ethanol and rinsed with triply distilled water, followed by 10 min in 0.5 M NaOH in 10% H_2O_2 and 30 min in water at 90 °C. The slides were dried under a stream of purified air. The freshly cleaned slides were coated with 1000 Å gold in a cryo-HV evaporator (Key High Vacuum) equipped with a Maxtek TM-100 thickness monitor. Homogeneous deposition was obtained by rotation of the substrate plate at moderate speed. The gold (99.99%) was evaporated from a tungsten boat at $\approx 10^{-6}$ Torr, at a deposition rate of 1 Å s^{-1}. The gold-covered slides were annealed in air at 255 °C for 168 min. The heating rate was 5 °C min^{-1}, and the slides were left to cool to ambient temperature.

Monolayer preparation: The gold substrates were pretreated in mild oxygen plasma (2.5 mA, 1–10 mbar for 2 min) in an Edwards S150B sputter coater and then immersed in ethanol for 10 min (to remove the oxide layer [9]).

Preparation of THB-Ala–Fe^{III} and THB-Leu–Fe^{III} monolayers: THB monolayers were adsorbed by immersion of gold substrates in a solution of 5 mM THB-Ala–Fe^{III} or THB-Leu–Fe^{III} in BCH:chloroform 4:1 (v/v) for 17 to 24 h. In certain cases subsequent adsorption of OM was carried out for 5 to 20 min from a solution of 2.0×10^{-2} M OM in BCH, to improve the blocking properties of the THB monolayers. The slides were then rinsed with dry chloroform, dried under a stream of clean air, rinsed with ethanol, and dried again with air.

Preparation of BHB-Ala–Cu^{II} monolayers: BHB-Ala–Cu^{II} monolayers were adsorbed by immersion of gold substrates in 5 mM BHB-Ala–Cu^{II} solution in BCH:chloroform 2:1 (v/v) for 17–24 h. When required, subsequent OM adsorption was carried out for ca. 20 min from a solution of 2.0×10^{-2} M OM in BCH followed by rinsing with chloroform and ethanol as above.

Chemical ion removal and rebinding: Removal of metal ions from THB and BHB monolayers was carried out by immersion of the electrodes for 2 h in 0.6 mM aqueous solution of Na_2-EDTA. Rebinding of metal ions to the ligand monolayers involved immersion in solutions containing a binding ion. For readsorption of Fe^{3+}, the electrodes were immersed in a solution of 5 mM $Fe_2(SO_4)_3$ in acetate buffer (pH = 4) for 10 min and then dipped in stirred water for 15 min. The use of acetate buffer (pH = 4) is dictated by the pH requirements: More acidic solutions would shift the hydroxamates to the protonated form, thus inhibiting complex formation, while basic solutions promote precipitation of iron hydroxide.

Ellipsometry: A Rudolph Research Auto-EL IV null ellipsometer with a tungsten–halogen light source was used, at an angle of incidence $\phi = 70°$ and a wavelength $\lambda = 6328$ Å. The same three points were measured with the bare and monolayer-covered slides. The thicknesses of THB and BHB monolayers were calculated by using a film refractive index of $n_f = 1.45$, $k_f = 0$, i.e., assuming a transparent film. The accuracy of the ellipsometric thickness measurement for a certain monolayer is ±1 Å.

Contact angle (CA) measurements: CAs were measured with a telescope goniometer (Rame–Hart 100) at an accuracy of ±2°. The liquid used for CA measurements was

0947-6539/96/0207-0760 $ 15.00+.25/0 Chem. Eur. J. 1996, 2, No. 7

water; the two organic solvents usually used (BCH and HD) wet THB and BHB monolayers completely.

Electrochemical measurements: *Cu underpotential deposition (UPD)*: The electrode coverage by THB and BHB monolayers (*without* OM) was measured using Cu UPD [10]. The fraction of gold surface covered by these monolayers was determined by comparing the amount of charge required for Cu UPD at an Au/monolayer electrode with that for a bare Au electrode of the same geometric area, obtained by integration of the respective cathodic UPD peaks. The accuracy of the UPD coverage measurements is estimated at ±5%. The Cu UPD was carried out by cyclic voltammetry in 1 mM $CuSO_4$ +0.1 M Na_2SO_4 solution in the range +0.400 to −0.400 V vs. mercurous sulfate reference electrode (MSE, +0.400 V vs. KCl-saturated calomel electrode), using a Solartron–Schlumberger model 1286 potentiostat and a Huston 100 x–y recorder. The electrodes were cycled at 100 mVs^{-1}.

AC-impedance spectroscopy: The AC-impedance measurements were performed with a conventional three-electrode cell with a MSE reference electrode and a platinum disk counter electrode. A Solartron–Schlumberger model 1286 potentiostat was used with model 1250 frequency response analyzer. The impedance was measured at seven discrete frequencies per decade, in the range 0.1 Hz to 65 kHz, at an amplitude of 5 mV (rms). The measurements were performed in 0.1 M Na_2SO_4 (i.e., supporting electrolyte only), at a fixed potential of 0.300 V (vs. MSE). The results were presented as complex-plane ("Nyquist") plots using the complex capacitance presentation [11]. Quantitative analysis was carried out using the software package Equivalent Circuit (B. A. Boukamp, University of Twente, The Netherlands).

Preparation of $CH_2{=}CHCH_2OCH_2C(Et)(CH_2OH)_2$ (2B, Scheme 1): EtC-$(CH_2OH)_3$ (67 g, 0.5 mol) was suspended in H_2O (75 mL) and treated dropwise with 4 N NaOH (42 mL) and subsequently allyl alcohol (0.75 mL). The resulting suspension was heated to 75 °C and was treated dropwise with allyl bromide (14.45 mL, 0.167 mol) and stirred for 2 h at the same temperature. The suspension was then filtered, and the filtrate washed with toluene and concentrated. Purification by flash chromatography (1–4% MeOH–CH_2Cl_2) afforded 16.6 g (19%) product. ^{1}H NMR ($CDCl_3$): δ = 5.72 (m, 1H; CH_2CH), 5.20 (m, 2H; CH_2CH), 3.97 (d, 2H; $CHCH_2O$), 3.70 (s, 4H; CH_2OH), 3.46 (s, 2H; OCH_2C), 1.25 (q, 2H; CH_2{Et}), 0.84 (t, 3H; CH_3{Et}).

Preparation of $CH_2{=}CHCH_2OCH_2C(Et)(CH_2OCH_2COOC_6Cl_5)_2$ (3B):
$CH_2{=}CHCH_2OCH_2C(Et)(CH_2OCH_2COOEt)_2$: Compound **2B** (8.3 g, 47.7 mmol) was dissolved in dry CH_2Cl_2 (100 mL), cooled to 0 °C, and then treated with $BF_3{\cdot}Et_2O$ (10 drops) and stirred for 30 min. Then $N_2CHCOOEt$ (18 mL, 0.166 mol) was added dropwise, and the solution stirred 30 min at 0 °C and 2 h at RT. The reaction mixture was washed with water, 1 N $NaHCO_3$, and again water, dried with Na_2SO_4, and concentrated. Purification by flash chromatography (0–20% EtOAc/*n*-hexane) yieled 8.37 g (51%) product. IR ($CDCl_3$): $\tilde{\nu}$ = 1750.1 cm^{-1}; ^{1}H NMR ($CDCl_3$): δ = 5.88 (m, 1H; CH_2CH), 5.18 (m, 2H; CH_2CH), 4.21 (q, 4H; CH_2CH_3), 4.07 (s, 4H; CH_2OCH_2), 3.98 (d, 2H; $CHCH_2O$), 3.62 (s, 4H; CH_2OCH_2), 3.53 (s, 2H; OCH_2C), 1.49 (q, 2H; CH_2{Et}), 1.27 (t, 6H; CH_2CH_3), 0.90 (t, 3H; CH_3{Et}).

$CH_2{=}CHCH_2OCH_2C(Et)(CH_2OCH_2COOH)_2$: Diester $CH_2{=}CHCH_2OCH_2C$-(Et)$(CH_2OCH_2COOEt)_2$ (4.41 g, 12.7 mmol) was dissolved in MeOH (30 mL) and treated with 2 N KOH (15 mL). The solution was heated to 70 °C for 2 h, then cooled and acidified with HCl to pH ≈ 1.5. The mixture was extracted with ethyl acetate (180 mL). Evaporation of the solvent afforded 3.59 g (98%) of the diacid. IR ($CDCl_3$): $\tilde{\nu}$ = 1717 cm^{-1}; ^{1}H NMR ($CDCl_3$): δ = 5.87 (m, 1H; CH_2CH), 5.23 (m, 2H; CH_2CH), 4.10 (s, 4H; CH_2OCH_2), 3.99 (d, 2H; $CHCH_2O$), 3.50 (s, 4H; CH_2OCH_2), 3.39 (s, 2H; OCH_2C), 1.46 (q, 2H; CH_2{Et}), 0.87 (t, 3H; CH_3{Et}).

$CH_2{=}CHCH_2OCH_2C(Et)(CH_2OCH_2COOC_6Cl_5)_2$: A cooled (0 °C) solution of diacid $CH_2{=}CHCH_2OCH_2C(Et)(CH_2OCH_2COOH)_2$ (3.68 g, 12.7 mmol), DMAP (1.55 g, 12.7 mmol), and C_6Cl_5OH (7.44 g, 27.94 mmol) in dry CH_2Cl_2 (100 mL) was treated with DCC (5.76 g, 27.94 mmol). The solution was stirred for 1 d at room temperature, and the resulting DCU precipitate was filtered. The filtrate was concentrated and purified by flash chromatography ($CHCl_3$) to afford 4.6 g (35%) of the product **3B**. IR ($CDCl_3$): $\tilde{\nu}$ = 1802 cm^{-1}; ^{1}H NMR ($CDCl_3$): δ = 5.86 (m, 1H; CH_2CH), 5.17 (m, 2H; CH_2CH), 4.47 (s, 4H; CH_2OCH_2), 3.97 (d, 2H; $CHCH_2O$), 3.78 (s, 4H; CH_2OCH_2), 3.56 (s, 2H; OCH_2C), 1.45 (q, 2H; CH_2{Et}), 0.90 (t, 3H; CH_3{Et}).

Preparation of $CH_2{=}CHCH_2OCH_2C(Et)[CH_2OCH_2CONHCH(CH_3)CON-(OCOPh)CH_3]_2$ (7B-COPh): A solution of **3B** (4.27 g, 5.39 mmol) and $H_2NCH(CH_3)CON(OH)CH_3$ (**6**) [5a] (1.52 g, 12.93 mmol) in dry CH_2Cl_2 (20 mL) was stirred 2 d at room temperature (pH ≈ 8 maintained by addition of Et_3N). The reaction mixture was concentrated and dissolved in dry $CHCl_3$ (20 mL). DMAP (1.57 g, 12.9 mmol) was added and the solution was cooled to 0 °C and treated with benzoyl chloride (1.83 mL, 23.7 mmol). After 1 h of stirring, the solution was diluted with $CHCl_3$, washed with water, dried over Na_2SO_4, and concentrated. Purification by flash chromatography (0–2% MeOH/CH_2Cl_2) afforded 3.72 g (77%) product. IR ($CDCl_3$): $\tilde{\nu}$ = 1771 (NOCOPh), 1667 cm^{-1} (CONH); ^{1}H NMR ($CDCl_3$): δ = 8.07 (m, 4H; ArH), 7.68 (m, 2H; ArH), 7.51 (m, 4H; ArH), 5.92 (m, 1H; CH_2CH), 5.22 (m, 2H; CH_2CH), 4.86 (m, 2H; CαH), 4.08 (m, 6H; CH_2OCH_2 + $CHCH_2O$), 3.62 (s, 4H; CH_2OCH_2), 3.54 (s, 2H; OCH_2C), 3.44 (s, 6H; NCH_3), 1.48 (q, 2H; CH_2{Et}), 1.33 (d, 6H; CαHCH_3)), 0.89 (t, 3H; CH_3{Et}).

Preparation of $BuS(CH_2)_3OCH_2C(Et)[CH_2OCH_2CONHCH(CH_3)CON-(OCOPh)CH_3]_2$ (8B-COPh): A degassed solution of **7B**-COPh (100 mg, 0.111 mmol), BuSH (35 mL, 0.333 mmol) and AIBN (15 mg) in toluene (2 mL) was heated for 24 h at 80 °C. The solution was concentrated and purified by PLC (preparative layer chromatography) (2% MeOH/$CHCl_3$) to afford 50 mg (45%) of product. IR ($CDCl_3$): $\tilde{\nu}$ = 1767 (NOCOPh), 1668 (CONH) cm^{-1}; ^{1}H NMR ($CDCl_3$): δ = 8.10 (m, 4H; ArH), 7.68 (m, 2H; ArH), 7.52 (m, 4H; ArH), 4.86 (m, 2H; CαH), 3.99 (ABq, 4H; CH_2OCH_2), 3.62 (ABq, 4H; CH_2OCH_2), 3.55 (m, 2H; CH_2OCH_2C), 3.53 (s, 2H; OCH_2C), 3.44 (s, 6H; NCH_3), 2.52 (m, 4H; CH_2SCH_2), 1.84 (m, 2H; CH_2CH_2O), 1.56 (m, 2H; $CH_3CH_2CH_2CH_2S$), 1.42 (m, 2H; CH_3CH_2), 1.36 (d, 6H; CαHCH_3), 1.45 (q, 2H; CH_2{Et}), 0.91 (t, 3H; CH_3CH_2), 0.84 (t, 3H; CH_3{Et}).

Deprotection and complexation of 8B (BHB-Ala): Compound **8B**-COPh (40 mg, 0.04 mmol) was dissolved in NH_3/MeOH solution (5 mL, 8.5% w/w) and stirred overnight. The solution was concentrated and purified by PLC ($CHCl_3$–3.5%MeOH) to yield 13 mg of **8B**. The compound was dissolved in $CHCl_3$ (4.5 mL), and a copper solution was added (4.5 mL of 3 mM $CuCl_2$–4 mM tris(hydroxymethyl)aminomethane in H_2O). After having been stirred for 30 min, the organic layer was separated, washed with water, dried over Na_2SO_4, and evaporated to give 7 mg of the copper complex. IR ($CDCl_3$): $\tilde{\nu}$ = 1675 (CONH), 1604 (CO-NO-Cu) cm^{-1}; FAB MS (free ligand): 581.3 (M + H)$^+$.

Preparation of $CH_2{=}CHCH_2OCH_2C(CH_2OH)_3$ (2T): Pentaeritritol (68 g, 0.5 mol) was suspended in H_2O (75 mL) and treated dropwise with 4 N NaOH (30 mL) and then allyl alcohol (0.75 mL). The resulting suspension was heated to 80 °C, treated dropwise with allyl bromide (10.8 mL, 0.125 mol), and stirred for 4 h at the same temperature. The suspension was then filtered, and the filtrate washed with toluene and concentrated. Purification by flash chromatography ($CHCl_3$–10% MeOH) afforded 9.57 g (11%) of product. ^{1}H NMR ($CDCl_3$): δ = 5.72 (m, 1H; CH_2CH), 5.20 (m, 2H; CH_2CH), 3.97 (d, 2H; $CHCH_2O$), 3.70 (s, 6H; CH_2OH), 3.46 (s, 2H; OCH_2C).

Preparation of $CH_2{=}CHCH_2OCH_2C(CH_2OCH_2COOC_6Cl_5)_3$ (3T):
$CH_2{=}CHCH_2OCH_2C(CH_2OCH_2COOEt)_3$: Compound **2T** was treated with $N_2CHCOOEt$ as described for **2B**. Purification of the crude material by flash chromatography (10–25% EtOAc/*n*-hexane) yieled 9.23 g (50%) of product. IR ($CDCl_3$): $\tilde{\nu}$ = 1750.1 cm^{-1}; ^{1}H NMR ($CDCl_3$): δ = 5.88 (m, 1H; CH_2CH), 5.18 (m, 2H; CH_2CH), 4.21 (q, 6H; CH_2CH_3), 4.07 (s, 6H; CH_2OCH_2), 3.98 (d, 2H; $CHCH_2O$), 3.62 (s, 6H; CH_2OCH_2), 3.53 (s, 2H; OCH_2C), 1.28 (t, 9H, CH_2CH_3).

$CH_2{=}CHCH_2OCH_2C(CH_2OCH_2COOH)_3$: The triester $CH_2{=}CHCH_2OCH_2C$-$(CH_2OCH_2COOEt)_3$ was hydrolyzed as described for the diester to provide 2.6 g (98%) of triacid. IR ($CDCl_3$): $\tilde{\nu}$ = 1717 cm^{-1}; ^{1}H NMR ($CDCl_3$): δ = 5.87 (m, 1H; CH_2CH), 5.23 (m, 2H; CH_2CH), 4.09 (s, 6H; CH_2OCH_2), 4.04 (d, 2H; $CHCH_2O$), 3.60 (s, 6H; CH_2OCH_2), 3.49 (s, 2H; OCH_2C).

$CH_2{=}CHCH_2OCH_2C(CH_2OCH_2COOC_6Cl_5)_3$: The triacid $CH_2{=}CHCH_2OCH_2C(CH_2OCH_2COOH)_3$ was converted to the corresponding trisphenolate as described for the dipodal analogue. Flash chromatography (CH_2Cl_2) of the crude material afforded 3.27 g (41%) of product. IR ($CDCl_3$): $\tilde{\nu}$ = 1802 cm^{-1}; ^{1}H NMR ($CDCl_3$): δ = 5.86 (m, 1H; CH_2CH), 5.17 (m, 2H; CH_2CH), 4.47 (s, 6H; CH_2OCH_2), 3.97 (d, 2H; $CHCH_2O$), 3.78 (s, 6H; CH_2OCH_2), 3.56 (s, 2H; OCH_2C).

Preparation of $CH_2{=}CHCH_2OCH_2C[CH_2OCH_2CONHCH(CH_3)CON-(OCOPh)CH_3]_3$ (7T-COPh): A solution of **3T** (3.97 g, 3.63 mmol) and $H_2NCH(CH_3)CON(OH)CH_3$ (**6**) (1.41 g, 11.97 mmol) in dry CH_2Cl_2 (20 mL) was stirred for 2 d at room temperature (pH ≈ 8 maintained by addition of Et_3N). The reaction mixture was concentrated and dissolved in dry $CHCl_3$ (20 mL). DMAP (1.33 g, 10.9 mmol) was added, and the solution was cooled to 0 °C and treated with benzoyl chloride (1.64 mL, 13.07 mmol). After 1 h of stirring, the solution was diluted with $CHCl_3$, washed with water, dried over Na_2SO_4, and concentrated. Purification by flash chromatography (0–2% MeOH/CH_2Cl_2) afforded 2.72 g (77%) of product. IR ($CDCl_3$): $\tilde{\nu}$ = 1771 (NOCOPh), 1667 (CONH) cm^{-1}; ^{1}H NMR ($CDCl_3$): δ = 8.07 (m, 6H; ArH), 7.68 (m, 3H; ArH), 7.51 (m, 6H; ArH), 5.92 (m, 1H; CH_2CH), 5.22 (m, 2H; CH_2CH), 4.86 (m, 3H; CαH), 4.08 (m, 8H; CH_2OCH_2 + $CHCH_2O$), 3.62 (s, 6H; CH_2OCH_2), 3.54 (s, 2H; OCH_2C), 3.44 (s, 9H; NCH_3), 1.36 (d, 9H; CαHCH_3).

Preparation of $BuS(CH_2)_3OCH_2C[CH_2OCH_2CONHCH(CH_3)CON(OCOPh)-CH_3]_3$ (8T-COPh): A degassed solution of **7T**-COPh (105 mg, 0.109 mmol), BuSH (35 mL, 0.327 mmol), and AIBN (15 mg) in toluene (2 mL) was heated for 24 h at 80 °C. The solution was concentrated and purified by flash chromatography (1% MeOH/$CHCl_3$) to afford 100 mg (87%) of product. IR ($CDCl_3$): $\tilde{\nu}$ = 1767 (NOCOPh), 1668 (CONH) cm^{-1}; ^{1}H NMR ($CDCl_3$): δ = 8.09 (m, 6H; ArH), 7.68 (m, 3H; ArH), 7.52 (m, 6H; ArH), 4.85 (m, 3H; CαH), 3.99 (ABq, 6H; CH_2OCH_2), 3.62 (ABq, 6H; CH_2OCH_2), 3.55 (m, 2H; CH_2OCH_2C), 3.53 (s, 2H; OCH_2C), 3.44 (s, 9H; NCH_3), 2.52 (m, 4H; CH_2SCH_2), 1.84 (m, 2H; CH_2CH_2O), 1.56 (m, 2H; $CH_3CH_2CH_2CH_2S$), 1.42 (m, 2H; CH_3CH_2), 1.36 (d, 9H; CαHCH_3), 0.91 (t, 3H; CH_3CH_2).

Deprotection and complexation of 8T (THB-Ala): Compound **8T**-COPh (100 mg, 0.094 mmol) was dissolved in NH_3/MeOH solution (5 mL, 8.5% w/w) and stirred overnight. The solution of **8T** was concentrated, redissolved in MeOH (5 mL), and $FeCl_3$ (11 mL of 60% w/w) was added. Solid NaOAc was added until pH 8 was reached. Separation by PLC ($CHCl_3$–3.5% MeOH) yielded 24 mg (31%) of the iron(III) complex. UV ($CHCl_3$): $\varepsilon = 2800$ (422 nm); CD ($CHCl_3$): $\Delta\varepsilon = +3.5$ (452 nm), -7.0 (372 nm); FAB MS (iron complex THB-Ala–Fe^{III}): 794.3 $(M + H)^+$.

Preparation of $BuS(CH_2)_3OCH_2C[CH_2OCH_2CONHCH(iBu)CON(OH)CH_3]_3$ (**8T**, R = *i*Bu; THB-Leu): The tripodal leucyl derivative was synthesized by similar procedures as the tripodal alanyl derivative. IR ($CDCl_3$): $\tilde{\nu} = 1668$ (CONH) cm^{-1}; ^1H NMR (CD_3OD): $\delta = 5.48$ (m, 3H; CαH), 4.02 (s, 6H; CH_2OCH_2), 3.64 (s, 6H; CH_2OCH_2), 3.53 (m, 4H; CH_2OCH_2C), 3.20 (s, 9H; NCH_3), 2.56 (t, 2H; CH_2S), 2.50 (t, 2H; CH_2S),1.82 (m, 2H; CH_2CH_2O), 1.54 (m, 11H; $CH_3CH_2CH_2CH_2S$, CH and CH_2{*i*Bu}), 1.42 (m, 2H; CH_3CH_2), 1.36 (d, 9H; CαHCH_3), 0.95 (m, 21H; CH_3CH_2, CH_3{*i*Bu}); FAB MS: 867.5 $(M + H)^+$, 889.5 $(M + Na)^+$.

Results and Discussion

Design and synthesis of monolayer components: The receptors for Fe^{3+}, $CH_3(CH_2)_3S(CH_2)_3OCH_2C[CH_2OCH_2CONHCHRCON(OH)CH_3]_3$, denoted THB-Leu (**8T**, R = *i*Bu) and THB-Ala (**8T**, R = Me) (Scheme 1), are composed of a biomimetic recognition site and a dialkyl sulfide immobilization tail, to promote self-assembly on gold surfaces. The design is based upon the natural ion binder ferrichrome as a model.[12] Ferrichrome, which strongly binds Fe^{3+} ions in solution, is a tripodal structure composed of a hexapeptide ring and three side chains that bear ion-binding hydroxamate groups. In our design,[5] the nonsymmetric tripodal ferrichrome structure is replaced with a C_3-symmetric one, and the chiral hexapeptide anchor is substituted by a tetrahedral carbon. The latter substitution causes a loss of asymmetric centers, which is compensated for by the introduction of chiral amino acids in the tripod chains between the anchor and the hydroxamate binding groups. An *n*-butyl group (rather than a hydrogen) is attached to the sulfur in order to improve the space filling between the bulky tripodal binding site and the gold substrate. The major features of our design are 1) a tetrahedral carbon as an anchor for the hydroxamate chains to allow the construction of tripodal or dipodal ion binders; 2) an exogenous functional group for attachment to the electrode surface; and 3) the amino acid bridges, which provide a wide choice of residues for adjustment of the cavity and its envelope. The effect of the amino acid bridge is demonstrated here with two derivatives, the leucyl derivative THB-Leu and the alanyl derivative THB-Ala, which seem to pack differently on the surface.

The design of these ion-binding molecules thus closely follows that of biomimetic ion carriers described earlier,[5, 13] with the addition of exogenously located thioethers for immobilization on gold surfaces. The synthetic schemes for the preparation of the present ion binders and their metal complexes were therefore also analogous to those for the earlier described binders.

The synthesis of THB and its Fe^{3+} complex THB–Fe^{III} involves four main transformations: 1) preparation of the functionalized tripodal structure as its triscarboxylate derivative; 2) preparation of the single-stranded hydroxamate; 3) coupling of the single-stranded hydroxamate with the tripodal structure to produce the trishydroxamate; and 4) binding of the alkyl sulfide group to the tripodal hydroxamate to produce the protected trishydroxamate. The Fe^{3+} complex THB–Fe^{III} is prepared upon hydrolytic removal of the benzoyl group followed by reaction with ferric chloride. The major synthetic steps are illustrated in Scheme 1. THB-Leu–Fe^{III} and THB-Ala–Fe^{III} were characterized by UV/CD spectroscopy, which indicated the predominance of the *Λ-cis* configuration.

The receptor for Cu^{2+}, $CH_3(CH_2)_3S(CH_2)_3OCH_2C(CH_2CH_3)[CH_2OCH_2CONHCH(CH_3)CON(OH)CH_3]_2$ (BHB-Ala), is similar in structure to THB, with one significant difference: The symmetry of the ion-binding cavity is changed from C_3 to C_2 by replacement of one of the hydroxamate chains with an ethyl group. The synthesis of BHB and its Cu^{II} complex was analogous to that of THB, as illustrated in Scheme 1.

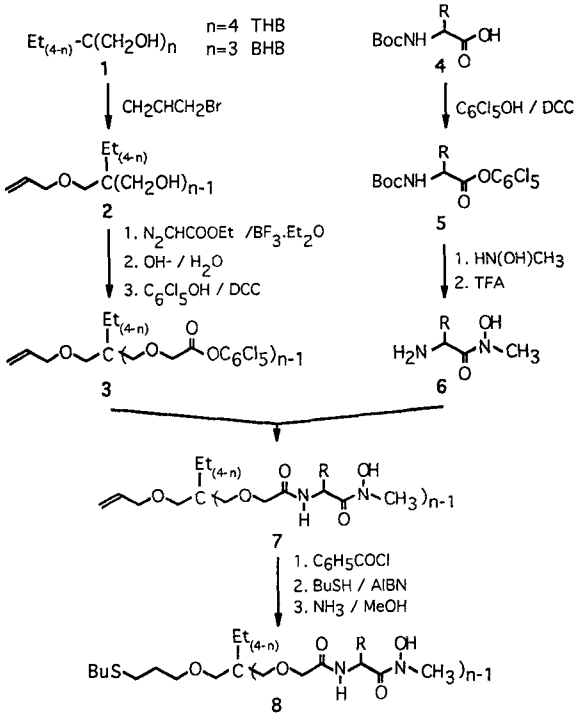

Scheme 1. Synthesis of the BHB binder **8B** ($n = 3$, R = CH_3) and THB binders **8T** ($n = 4$, R = CH_3 and *i*Bu).

All compounds were characterized by their spectroscopic data, which were analogous to those reported earlier for other biomimetic ion binders and in full agreement with the assigned structures.[5] The identities of the final products BHB-Ala, THB-Leu, and THB-Ala–Fe^{III} were further confirmed by their FAB mass spectra (see Experimental Procedure).

Wettability, thickness, and coverage measurements: The wettability of monolayer-covered surfaces can be correlated with monolayer structure.[14] Thus, advancing and receding contact angles (CAs) of water were measured for the ion-binding monolayers. The thickness of monolayers is also widely used as a test for monolayer quality, serving primarily to estimate molecular orientation in the monolayer. The theoretical thickness of the three monolayers (THB-Ala, THB-Leu, and BHB-Ala) is 15 Å when the molecules are fully extended and oriented perpendicular to the electrode surface.

The measured values of the coverage (from Cu UPD, see Experimental Procedure), ellipsometric thickness, and CAs are presented in Figures 2–4. The figures show results of a large number of experiments, as a visual indication of the extent of experimental reproducibility.

Figure 2 shows the relationship between the ellipsometric thickness and the measured monolayer coverage. The observed relationship may be rationalized by considering the fact that the ellipsometer measures an apparent average thickness over a macroscopic area. The apparent thickness would therefore be

0947-6539/96/0207-0762 $ 15.00+.25/0 Chem. Eur. J. 1996, 2, No. 7

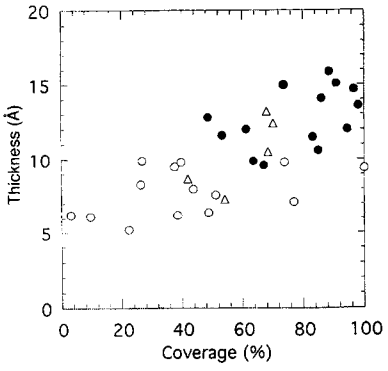

Fig. 2. Ellipsometric thickness vs. surface coverage (from Cu UPD) for THB-Ala–Fe^{III} monolayer (○), THB-Leu–Fe^{III} monolayer (●), and BHB-Ala–Cu^{II} monolayer (△) on gold.

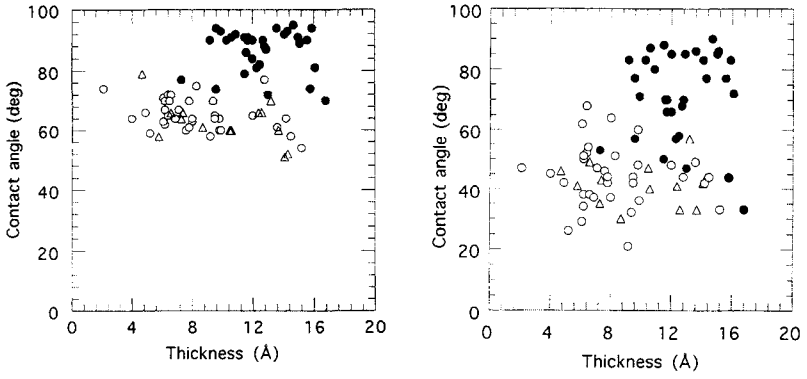

Fig. 3. Ellipsometric thickness vs. advancing water CAs (left) and receding water CAs (right) for the various monolayers on gold (same symbols as in Fig. 2).

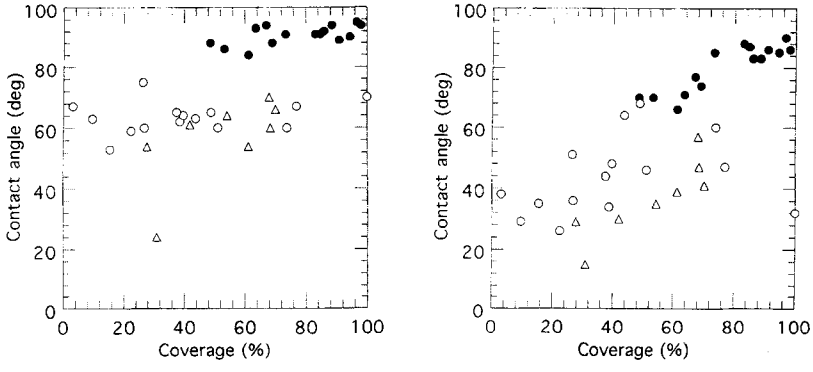

Fig. 4. Surface coverage (from Cu UPD) vs. advancing water CAs (left) and receding water CAs (right) for the various monolayers on gold (same symbols as in Fig. 2).

directly related to the extent of surface coverage by the monolayer.[15]

As seen in Figure 3 (left) and 4 (left), the advancing CAs for the three monolayers cover a relatively narrow range of values; the average CAs are summarized in Table 1. The advancing CAs are little affected by the coverage (Fig. 4, left) or the ellipsometric thickness (Fig. 3, left) of the monolayers, and are therefore of little use in characterizing these monolayers. On the other hand, the receding CAs increase with increasing thickness (Fig. 3, right) or coverage (Fig. 4, right), that is, the CA hysteresis (the difference between the advancing and receding CAs) is correspondingly decreased.

Table 1. Average advancing CAs of water for THB and BHB monolayers.

Monolayer	Adv. CA (H_2O)
THB-Ala	66±6
THB-Leu	85±7
BHB-Ala	61±6

The marked difference in the behavior of the advancing and receding CAs is characteristic of monolayer systems for which the value of the advancing CA for water is in the approximate range of 60–80°, that is, in the range of advancing CAs measured for "clean" gold surface in laboratory air. The CA hysteresis, on the other hand, is quite large (several tens of degrees) for bare gold with random contamination, but rather small (a few degrees) for well-organized monolayers; this would account for the results in Figures 3 and 4. It is therefore evident that meaningful CA characterization of such monolayers requires determination of both advancing and receding CAs, that is, the CA hysteresis.

The most apparent result in Figures 2–4 is the effect of the amino acid moiety in the ligand molecules (alanine or leucine) on the monolayer properties. This is evident from the fact that THB-Leu monolayers show values of advancing and receding CAs, ellipsometric thickness, and surface coverage that are quite different from those of THB-Ala and BHB-Ala monolayers. All the measured variables are distinctly higher with THB-Leu than with THB-Ala or BHB-Ala, which is usually indicative of a better organized monolayer.

The reason for the improvement in monolayer coverage and organization induced by the bulky *i*-butyl side chains is intriguing. It can be reasonably assumed that different side groups would have different intermolecular interactions and space-filling properties, resulting in different monolayer packing. Study of this aspect requires the use of other experimental tools, such as diffraction techniques and scanning probe microscopes, and is currently in progress.

AC-impedance measurements: As noted in the Introduction, AC-impedance spectroscopy provides an exceedingly powerful tool for determining the electrical nature of electrode systems,[6, 7] and was applied in the present work to the monolayer systems. The technique involves the application of a small-amplitude sinusoidal voltage to the working electrode, and the measurement of the magnitude and phase of the resulting current. The impedance can then be calculated at various modulation frequencies. The results are frequently presented as complex impedance plots, namely, the real (in-phase) plotted versus the imaginary (out-of-phase) components of the impedance at various frequencies. Analysis of the results is usually carried out by comparing the experimental results with those expected from a model electrical equivalent circuit, where the different elements in the equivalent circuit are assigned to actual components or processes of the physical system.

Monolayer systems on electrodes may be quite complex from the electrical point of view, as they comprise various resistors and capacitors corresponding to the solution, to the monolayer, and to the bare electrode (at pinholes). Hence, a full analysis of all the components in a wide frequency range would be advanta-

geous, in that it allows the various electrical elements to be separated and those whose variations are indicative of ion binding to the monolayer to be identified.

The impedance of THB and BHB monolayers on gold electrodes was measured in the frequency range 0.1–65000 Hz. In the present case the complex-capacitance (c plot) presentation was used to analyze the dispersion data; the complex capacitance C is defined as $1/j\omega Z$, where ω is the angular frequency and Z is the impedance.[11] We chose the c plot (rather than the usual z plot) representation, since RC (resistor, capacitor) elements in series are more conveniently analyzed by means of a c plot (semi-circle) than a z plot (straight line). In addition, the complex-capacitance presentation emphasizes the medium-to-low frequency region, where most of the relevant information is contained in the present case, and provides direct information regarding the out-of-phase component of the impedance.

AC measurements were performed after each step in the experimental procedure, that is, adsorption of an ion-binding monolayer, subsequent adsorption of OM to "seal" remaining pinholes,[16] chemical removal of the bound Fe^{3+} with EDTA, and rebinding of Fe^{3+} ions. The measurements were carried out in a solution containing supporting electrolyte only (0.1 M Na_2SO_4) at a potential of 0.300 V (vs. MSE), where no redox reaction occurs. The objective was to identify changes in the AC response, and hence in electrical properties (resistance, capacitance) of the monolayer, which can be assigned to the different stages. Of particular interest are changes that accompany ion binding and release and hence can be used for probing of ion binding.

Figures 5 and 6 present a series of experimental complex-capacitance plots of THB-Ala and THB-Leu monolayers on gold electrodes, corresponding to the different steps in the experimental procedure. Qualitatively, the main feature in the c plots is a distorted semi-circle at higher frequencies, corresponding to overlapping RC elements in series. At very low frequencies one observes a poorly defined element, which appears to be a process controlled by slow mass transport, which is rather irreproducible and assumed to be irrelevant to the present analysis. When the latter element is ignored, the total capacitance (C_t) after each step can be readily obtained as the diameter of the "semi-circle" (i.e., its extrapolated intercept with the real axis at the low-frequency end).

Examination of the AC results for the two monolayers (Figs. 5 and 6) shows a common trend in the capacitance values. C_t after adsorption is 12–13 $\mu F\,cm^{-2}$, compared with the value of ca. 20 $\mu F\,cm^{-2}$ for bare Au. After "sealing" with OM, C_t becomes significantly smaller (4–6 $\mu F\,cm^{-2}$). The next step (removal of the ions from the monolayer with EDTA) results in a further, moderate decrease of C_t, to ca. 4 $\mu F\,cm^{-2}$. The last step, namely, rebinding of Fe^{3+}, involves an increase of C_t to ca. 5.5 $\mu F\,cm^{-2}$.

The variations in C_t are consistent with the following qualitative considerations: The initial monolayer adsorption involves a decrease in the capacitance due to coverage of a large fraction of the electrode surface with the organic film. "Sealing" the bare spots (high double-layer capacitance) with OM (highly insulating layer) causes an additional marked decrease in the value of C_t. The next step (release of the ions by EDTA) results in a moderate decrease in C_t, assumed to be due to a change in the monolayer capacitance; although the complex is neutral, loss of the metal ion would result in a smaller dipole moment of the molecules and hence in a lower dielectric constant of the monolayer. The last step, rebinding of the metal ion, is the reverse of the previous step, and results in a moderate increase in C_t.

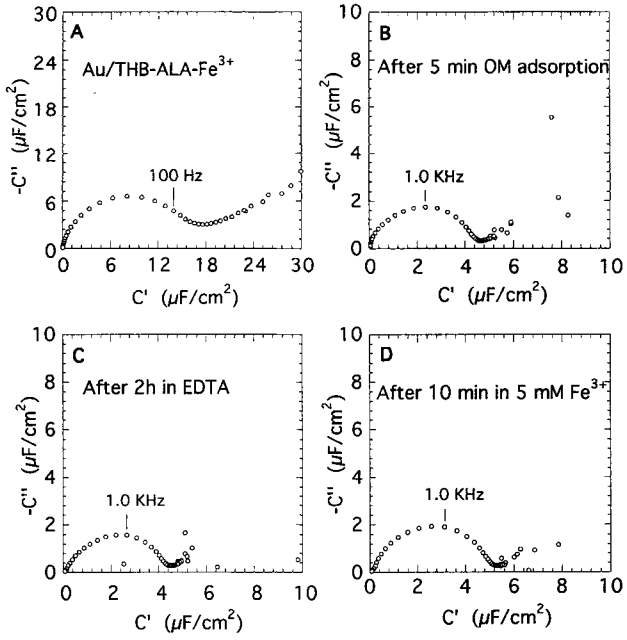

Fig. 5. Experimental c plots in 0.1 M Na_2SO_4 at 0.300 V (vs. MSE) for Au/THB-Ala electrode at different stages.

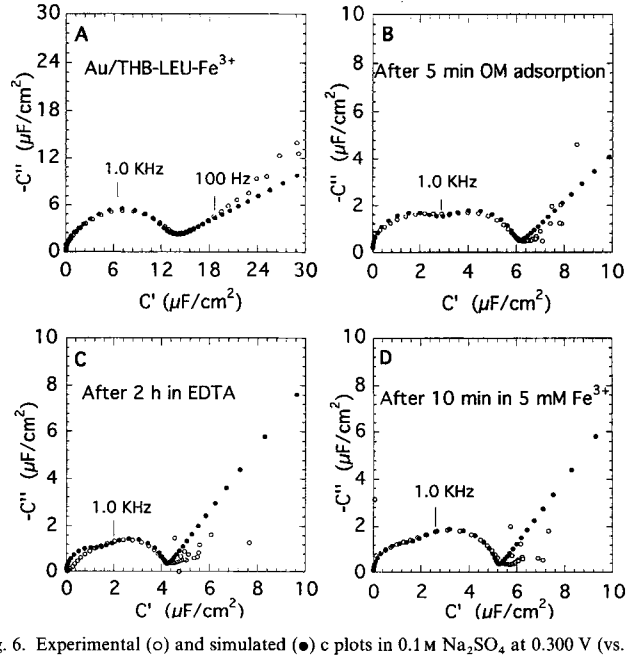

Fig. 6. Experimental (o) and simulated (•) c plots in 0.1 M Na_2SO_4 at 0.300 V (vs. MSE) for Au/THB-Leu electrode at different stages.

As noted above, the total capacitance C_t (not including the very low frequencies) is readily obtained with essentially no assumptions or models. Although one observes consistent changes in C_t which accompany Fe^{3+} binding and release, a more detailed analysis of the AC results may provide some insight and better accuracy. This is achieved by assigning a chosen electrical equivalent circuit to the system, and separating individual elements that change upon ion binding and release from those elements that do not. The AC results shown in Figure 6 were analyzed quantitatively by using the software package Equivalent Circuit (see Experimental Procedure). The package utilizes a nonlinear least-squares procedure to fit experimental AC dispersion data to an equivalent circuit model. All

0947-6539/96/0207-0764 $ 15.00+.25/0 Chem. Eur. J. 1996, 2, No. 7

the parameters in the model are adjusted simultaneously, and an optimal fit to the measured response is thus obtained. If the fit is not satisfactory, the model equivalent circuit is changed and the fitting procedure repeated.

Simulated curves produced by the fitting procedure are also shown in Figure 6. The model equivalent circuit used to fit the experimental data is shown in Figure 7. It comprises a solution resistor R_s, a parallel combination of two series RC circuits (R_IC_I and $R_{II}C_{II}$), and a diffusionlike element Q, which has the form of a constant phase element (CPE).[17] As discussed above, Q is assigned to a parasitic diffusion-controlled process, which appears at very low frequencies as a near-Warburg element and has no bearing on the present discussion.

Table 2 presents the values of the parameters in the equivalent circuit shown in Figure 7, obtained by the computer best-fit procedure at the different stages. Two points should be noted: 1) In the discussion below we ignore the values of the low-frequency element Q (Y and n);[6] the values are given for the sake of completeness. 2) The value of R_s (the solution resistance) evidently remains essentially constant during all the steps, since this element is not related to the factors changed during the experiments.

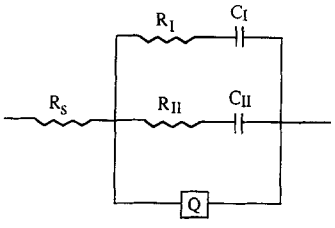

Fig. 7. The electrical equivalent circuit used to analyze the experimental impedance spectrum in Fig. 6.

As seen in Table 2, the branch that changes most upon removal and rebinding of Fe^{3+} ions is R_{II},C_{II}. This identification provides several advantages: 1) It presents an additional element (R_{II}) that may be determined and used to probe ion binding to the monolayers. 2) It indicates that most of the change in C_t related to ion binding reflects changes in the element C_{II}. The latter implies that the use of C_{II} (rather than C_t) for probing ion binding and release would improve the accuracy; while C_t changes by ca. 33% and 25%, respectively, upon Fe^{3+} removal and rebinding (calculated from Fig. 6), C_{II} changes by 45% and 44%, respectively (calculated from Table 2).

Table 2. Calculated parameters from computer fitting (normalized to the electrode geometric area) using the equivalent circuit in Fig. 7 for the THB-Leu monolayer system at different stages. The simulated curves are shown in Fig. 6.

	THB	OM	EDTA	Fe^{3+}
R_s (Ωcm^2)	13.0	13.0	13.0	13.0
R_I (Ωcm^2)	37.2	204	204	96.5
C_I ($\mu F cm^{-2}$)	5.4	2.5	2.3	2.5
R_{II} (Ωcm^2)	0	0	12	0
C_{II} ($\mu F cm^{-2}$)	5.5	3.3	1.8	2.6
Y ($10^{-6}\,\Omega^{-1} cm^{-2}$)	18	4.5	4.1	3.1
n	0.68	0.50	0.40	0.49

It is of interest, though somewhat speculative, to attach physical meaning to the two capacitive branches. With a few exceptions (discussed below), Table 2 indicates that the R_{II},C_{II} branch changes significantly in the last two steps (ion release and rebinding, as detailed above), whereas the R_I,C_I branch changes significantly in the first step (OM adsorption). It may therefore be assumed that R_{II},C_{II} represents the fraction of the electrode covered with THB monolayer, while R_I,C_I represents the fraction of the electrode exposed to the solution (pinholes in the THB monolayer), which is "sealed" with OM in the first step. It is important to note here that the values in Table 2 are normalized to the electrode (geometric) area, since the individual fractional areas associated with the two RC branches have not been determined. Therefore, it is the *changes* in the various parameters that are significant, rather than the absolute numbers.

In what follows, the changes in the values of the four elements in the capacitive branches are discussed in light of the suggested assignment. Although, as noted above, we do not at this point have independent evidence to support this model, it is of interest to test to what extent it may indeed describe the physical system and what are its limitations.

The value of R_I following THB-Leu adsorption is not readily understood; if this element indeed represents the resistance at uncovered areas (pinholes), one would not expect an additional resistive element in series with the solution resistance. The value is, however, exaggerated, owing to the fact that the fraction of pinholes is presumably small, which was not considered in the calculation (see above). It is possible that the finite value of R_I represents areas of random adsorption of THB, or certain surface contamination. In the next step, adsorption of OM, the OM molecules seem to replace the THB (or contamination) at imperfect adsorption sites, and the situation becomes better defined. R_I increases substantially, as it now represents the resistance of a highly blocking monolayer. In the third step (Fe^{3+} removal) the value of R_I remains constant, as this step does not affect the OM fraction. During the last step (rebinding of Fe^{3+}) the value of R_I unexpectedly decreases; this may indicate a certain restructuring of the monolayer upon ion rebinding in Fe^{3+} solution.

Regarding the parameter C_I, the decrease from 5.4 to 2.5 $\mu F cm^{-2}$ cannot be explained by simple OM filling of bare spots, as the capacitance of an OM-covered electrode is lower than that of bare Au by more than an order of magnitude.[18] The value after THB adsorption may therefore be attributed to the poorly defined situation noted above for R_I at that stage, while the decrease in C_I during OM adsorption is attributed to the low capacitance of the OM monolayer. In the last two steps the value of C_I remains essentially unchanged, as these steps do not involve the OM fraction.

The parameter R_{II} is assumed to represent the resistance assigned to the THB fraction of the monolayer. Its value is zero within the accuracy of the parameter fit (i.e., much smaller than R_s) during the first two stages. It increases substantially upon removal of the bound ion, and decreases again to a very small value upon rebinding of Fe^{3+}. These results are rather intriguing, as they may suggest that the presence of a bound metal ion substantially increases the probability of electron tunneling through the monolayer.

The element C_{II} is assumed to represent the capacitance of the THB-Leu monolayer. Its value decreases after "sealing" with OM, possibly due to exchange of parts of the THB monolayer with OM. The variations in C_{II} during the next three steps appear to be indicative of Fe^{3+} removal and rebinding: The decrease in C_{II} upon removal of the metal ion would result from a decrease in the monolayer polarity and hence its dielectric constant, while rebinding of the ions reverses the situation.

This discussion may be summarized by stating that the assignment of the two capacitive branches to certain parts of the monolayer system appears adequate most of the time, but in some cases deviations are observed that need to be explained. The bottom line is, however, that the AC results show clear changes in measurable parameters at different stages of the experiment.

Conclusions

A new family of monolayer-forming ion binders has been presented, based upon the natural ion binder ferrichrome as a model and hydroxamates as coordinating groups. These ion binders self-assemble on smooth gold electrodes to form monomolecular layers of defined thickness, contact angles (for water), and surface coverage. A key element in the design of the new binders is their modular assembly and the separation between the ion-binding cavity and the attachment site to the gold. The modular assembly allows control over the cavity symmetry, size, and envelope, by controlling the anchor's symmetry (C_2 vs. C_3), and the nature of the amino acids (α-, β-, or γ-amino acid) and their side groups (*i*-butyl, methyl). This "coarse tuning" can be supplemented by "fine tuning" through the choice of guest ion and the molecular matrix created upon self-assembly of the preformed metal complex. The design allows the molecules to be optimized in terms of specific ion binding and packing on the gold surface. Higher coverage, CAs, and ellipsometric thickness are obtained with molecules that contain bulky, hydrophobic side groups (*i*-butyl); this may be explained by better space filling, hydrophobic interactions, or both. The origin of this intriguing observation is currently the subject of experimental and theoretical investigations.

The AC-impedance response of organic monolayers was shown to be a useful tool for the investigation of monolayer systems, when applied in a wide frequency range. It presents several advantages over voltammetry: 1) the very small voltage perturbation, which implies minimal structural alteration of the monolayer; and (2) the possibility of extracting the required information in the presence or absence of a redox reaction. Impedance spectroscopy provides a comprehensive electrical picture of the electrode/monolayer/solution interphase, and can be used to follow changes in the monolayer. In the present case, the system has been modeled by using a single electrical equivalent circuit. Although parts of the AC response are not yet understood, electrical elements (R_{II} and C_{II}) have been identified that appear to be indicative of ion binding and release, and can therefore be used to probe such procresses. Moreover, once these elements have been identified and their characteristic time constant $\tau = R_{II}C_{II}$ determined, it becomes possible to monitor changes in the impedance at a single frequency (in the vicinity of τ^{-1}) for ion sensing. This would simplify considerably the performance of routine measurements.

Impedance spectroscopy can be effective and useful in probing a variety of other processes in monolayers and multilayers on metal substrates, and therefore has the potential of becoming an important experimental tool in monolayer research.

Acknowledgment: Support of this work from the Minerva Foundation, Munich, Germany (A. S. and I. R.) and from the New Energy Development Organization (NEDO), Japan (I. R.) is gatefully acknowledged. A. S. is holder of the Siegfried and Irma Ullman Professorial Chair.

Received: October 23, 1995 [F230]

[1] a) A. Ulman, *Introduction to Ultrathin Organic Films*, Academic Press, NY, **1991**. b) L. H. Dubois, R. G. Nuzzo, *Ann. Rev. Phys. Chem.* **1992**, *43*, 437. c) R. H. Tredgold, *Order in Thin Organic Films*, Cambridge University Press, Cambridge, **1994**, pp. 116–134.
[2] C. Duschl, M. Liley, H. Vogel, *Angew. Chem. Int. Ed. Engl.* **1994**, *33*, 1274.
[3] a) I. Rubinstein, S. Steinberg, Y. Tor, A. Shanzer, J. Sagiv, *Nature* **1988**, *332*, 426. b) S. Steinberg, Y. Tor, E. Sabatani, I. Rubinstein, *J. Am. Chem. Soc.* **1991**, *113*, 5176. c) S. Steinberg, I. Rubinstein, *Langmuir* **1992**, *8*, 1183. d) S. Steinberg, Y. Tor, A. Shanzer, I. Rubinstein, in *Thin Films, Organic Thin Films and Surfaces* (Ed.: A. Ulman), Academic Press, NY, **1995**, Vol. 20.
[4] a) G. Winkelmann, D. van der Helm, J. B. Neilands, *Iron Transport in Microbes, Plants and Animals*, VCH, Weinheim, **1987**. b) J. B. Neilands, *Struct. Bonding* **1984**, *58*, 1. c) K. N. Raymond, G. Mueller, B. F. Matzanke, *Top. Curr. Chem.* **1984**, *123*, 49. d) R. C. Hider, *Struct. Bonding* **1984**, *58*, 25.
[5] a) I. Dayan, J. Libman, Y. Agi, A. Shanzer, *Inorg. Chem.* **1993**, *32*, 1467. b) Y. Tor, J. Libman, A. Shanzer, *J. Am. Chem. Soc.* **1987**, *109*, 6518. c) H. Weizman, M. Sc. Thesis, Weizmann Institute, **1993**. d) Y. Agi, Ph.D. Dissertation, Weizmann Institute, **1994**.
[6] J. R. Macdonald (Ed.), *Impedance Spectroscopy*, Wiley, NY, **1987**.
[7] C. Gabrielli, in *Physical Electrochemistry: Principles, Methods and Applications*, (Ed.: I. Rubinstein), Marcel Dekker, NY, **1995**.
[8] M. Stelzle, G. Weissmüller, E. Sackmann, *J. Phys. Chem.* **1993**, *97*, 2974.
[9] H. Ron, I. Rubinstein, *Langmuir* **1994**, *10*, 4566.
[10] a) A. B. Christie, *Methods of Surface Analysis*, (Ed.: J. M. Walls), Cambridge University Press, **1990**, Chap. 5. b) D. M. Kolb, in *Advances in Electrochemistry and Electrochemical Engineering*, (Eds.: H. Gerischer, C. W. Tobias), Wiley, NY, **1978**, Vol. 11.
[11] I. Rubinstein, E. Sabatani, J. Rishpon, *J. Electrochem. Soc.* **1987**, *134*, 3078.
[12] T. Emery, *Biochemistry* **1971**, *10*, 1483.
[13] Y. Shechter, A. Shisheva, R. Lazar, J. Libman, A. Shanzer, *Biochemistry* **1992**, *31*, 2063.
[14] See e.g. ref. [1a], pp. 283–286.
[15] The non-zero intercept in Fig. 2 appears to be due primarily to the fact that "bare" gold surface is covered by physisorbed organic contaminations.
[16] The OM adsorption step [3a] was added in this part in order to simplify the impedance measurements by providing a high surface coverage, as discussed in the text.
[17] The admittance representation of a CPE is given by: $Y(\omega) = Y_0(j\omega)^n$, where Y_0 and n are adjustable parameters and ω is the angular frequency; see e.g. ref. [7], pp. 39, 77.
[18] a) E. Sabatani, I. Rubinstein, R. Maoz, J. Sagiv, *J. Electroanal. Chem.* **1987**, *219*, 365. b) E. Sabatani, I. Rubinstein, *J. Phys. Chem.* **1987**, *91*, 6663.

0947-6539/96/0207-0766 $ 15.00+.25/0